Confinement of spherical colloid particles in a soft fluid membrane tube*

Zheng Bin(郑 斌) and Meng Qing-Tian(孟庆田)†

College of Physics and Electronics, Shandong Normal University, Jinan 250014, *China*

(Received 13 August 2013; revised manuscript received 21 September 2013; published online 24 January 2014)

We investigate the structure of multiple spherical particles confined in a soft membrane tube that originally has a cylindrical shape. Assuming an attraction energy between the surface of the spherical particle and the inner wall of the membrane tube, we show that a variety of conformational structures can be stabilized on the basis of analyzing a Helfrich energy for the soft tube. Using a numerical approach, we calculate the phase diagram in terms of basic parameters in the system. Structures that prefer close contact of spheres and structures that contain well separated spheres are found in this calculation.

Keywords: membrane, Helfrich model

PACS: 87.15.ad, 87.15.kt, 68.35.Np **DOI:** 10.1088/1674-1056/23/3/038701

1. Introduction

Recent experimental efforts have been made to stabilize long tubular fluid membranes by using a number of experimental techniques.[1–8] These soft tubes can be used as a playground for further exploitation of their physical properties, mixed with other molecules. Experimental reports are available on the possibilities of using the tubular membrane to confine DNA molecules, latex particles, and even bacteria.[9–11] Theoretical and computer-simulation studies have indicated interesting structures and phase behavior induced by the mutual interaction between the confined molecules and the soft wall of the tube.[12–18] In this paper, we theoretically consider the phase behavior of multiple spherical particles confined in an originally cylindrical soft tube.[11] The properties of a single or double sphere(s) confined in a tube were reported in a Letter written by Chen *et al*;[15] the report shows that for a single spherical particle in a tube, two phases exist which can be divided by the contact angle, while for two spherical particles confined in the tube, three phases exist that can be characterized by the contact angle and the inter-sphere distance. However, close scrutiny shows that for the latter case, since the inner contact angle is also a geometrical parameter, just as the outer wrapping angle does, there maybe also another phase curve that exists in the phase characterized by nonzero inner contact angel and zero inter-sphere distance. Therefore, we focus on the missing phase curve and the behavior of multiple spherical particles in this work.

To model the fluid membrane, we use the Helfrich model that contains two parameters: the bending rigidity κ and surface tension σ.[19,20] By taking a cylindrical membrane segment, it is well known that we can relate the radius of the tube, a, with these two parameters from a simple analysis of the energy function.[12] It is also possible to show that the model yields an extracted tube by considering a pulling force on a "pick-up" point of an originally much larger flat sheet.[21] In this paper, we focus on a membrane tube segment connected to a pulling device remotely on one side and a reservoir of membrane molecules (for example, a lipid bilayer vesicle) remotely on the other side. It is not uncommon in actual experimental setups where the extraction of a tubular membrane requires a much larger vesicle as the "reservoir";[1–6] the tube has open ends where "membrane material" can be fed or taken away. The idealized tube segment considered in this work is assumed to be far from the source; for such a system, σ is a well-defined parameter.

We consider spheres that have a radius R moving inside the membrane tube. The basic theoretical ingredients in the current model follow the same flavor that has been used in recent studies of other membrane-particle adhesion problems. The Helfrich energy is parameterized in an axisymmetric coordinate system by a shape function so that the mathematical problem can be mapped into a classical Hamiltonian dynamics problem.[22] Beyond the membrane function, an adhesion energy per unit area between the membrane and the particle, w, is assumed as another basic parameter. It is not hard to see that there are only two dimensionless reduced parameters in such a model: wR^2/κ and $\sigma R^2/\kappa$. Adhesion (or adsorption) of a single or multiple spherical particle(s) in an axisymmetric conformation, shown in Fig. 1, is then considered. The total energy of the system, minimized by taking into consideration the different shapes and configurations of the particles, is identified as the stable state. The setup of the current model is similar to other interacting systems between a soft membrane surface and a rigid surface in various geometrical arrangements, on

*Project supported by the National Natural Science Foundation of China (Grant No. 11074151).

†Corresponding author. E-mail: qtmeng@sdnu.edu.cn

© 2014 Chinese Physical Society and IOP Publishing Ltd

which a large amount of theoretical work has been carried out recently.[15,23–32]

This paper is organized as follows. In Section 2, we lay out the theoretical framework together with the adopted numerical approach. In Subsection 3.1, we discuss the new structure characterized by nonzero inner contact and focus on the phase diagram of two particles confined in a tube, where we pay attention to the discussion of physical properties that can be used to distinctively identify the multiphase behavior of the system. In Subsection 3.2, we generalize the results from Subsection 3.1 and discuss the phase diagram of an N particle system. In the last paragraph of the summary section, Section 4, some possible experimental probes to verify the theoretical prediction in this paper are suggested.

2. Model

We assume that the membrane tube is already extracted from a much larger remote membrane reservoir, which by itself could be a closed vesicle as in most experimental settings. The segment of tube membrane that we are interested in can change its total area, drawing lipid molecules from the much larger reservoir if necessary to change its total area.[1–6] Without the inclusion of spherical particles, the shape of the tube is a perfect cylinder with radius a.

We use a phenomenological energy model to describe the deformable region of the membrane tube[33,34]

$$E = \int \mathrm{d}A(2\kappa K^2 + \sigma). \tag{1}$$

The first term inside the brackets describes the energy cost of bending an area element into a curved surface that has a mean curvature K, where the coefficient κ has the energy units representing an energy penalty of bending.[19,20] Because the tube segment is part of a larger, closed system, the Gaussian curvature term has no overall effects hence has been removed from the above expression.[33,34] Furthermore, we assume that there is no intrinsic asymmetry reason from the constituting molecules in the membrane to produce a so-called spontaneous curvature. The second term originates from the energy cost of stretching (or compressing) the surface element, associated with a surface tension σ needed for the consideration of a changing total area. One can show through a simple minimization argument that for a free tube, the membrane adopts a cylindrical shape with radius

$$a = \sqrt{\kappa/2\sigma}, \tag{2}$$

which sets a length scale for the current problem.[12]

Adopting the co-axial coordinate frame shown in Fig. 1, we see that the conformation of the membrane can be described by a single shape function $\psi(s)$, where s is an arc variable describing the location of the curve. Both $r(s)$ and $z(s)$ can be related to $\psi(s)$ through the relationship

$$\frac{\mathrm{d}r}{\mathrm{d}s} = -\sin\psi(s), \tag{3}$$

$$\frac{\mathrm{d}z}{\mathrm{d}s} = \cos\psi(s). \tag{4}$$

For the un-adhered part of the membrane tube, the energy in Eq. (1) then takes the form

$$E_{\mathrm{free}} = 4\pi \int_0^S \mathrm{d}s r \left\{ \frac{\kappa}{2}\left[\frac{\mathrm{d}\psi}{\mathrm{d}s} + \frac{\cos\psi}{r}\right]^2 + \sigma \right\}, \tag{5}$$

where $s = 0$ is the contact point of the membrane and the particle. A prefactor of 2 has been included to account for two segments of the non-adhering membrane, to the right- and left-hand sides of the sphere.

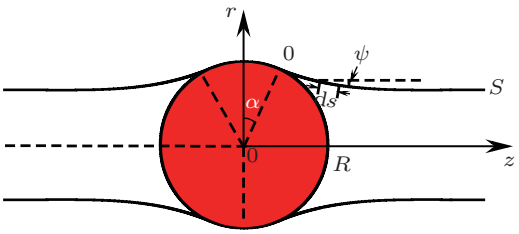


Fig. 1. (color online) Cross-section illustration of a rigid spherical particle (red) of radius R wrapped inside a soft membrane tube that was originally a right circular cylinder of radius a ($R > a$ or $R < a$). The coordinate system used for theoretical calculation assumes a co-axial setting where the cross-section view coinciding with the original cylinder axis is shown.

Over the total arclength S, the deformed tube segment spans the range $[z(0), z(S)]$ in the z direction, where

$$z(S) - z(0) = \int_0^S \frac{\mathrm{d}z}{\mathrm{d}s}\mathrm{d}s = \int_0^S \cos\psi(s)\mathrm{d}s. \tag{6}$$

Each segment of the original, undisturbed elastic tube has an energy $2\pi\sqrt{2\sigma\kappa}[z(S) - z(0)]$; taking both segments into consideration and using the undisturbed energy as the reference, we arrive at the energy difference

$$\Delta E_{\mathrm{free}}[\psi(s)] = E_{\mathrm{free}}[\psi(s)] - 4\pi \int_0^S \mathrm{d}s\sqrt{2\sigma\kappa}\cos\psi. \tag{7}$$

The energy functional ΔE_{free} needs to be minimized with respect to $\psi(s)$, which is subject to the boundary conditions

$$\psi(0) = \alpha, \tag{8}$$

$$\psi(S) = 0, \tag{9}$$

where α is the wrapping angle defined in Fig. 1.

Using the sphere radius R as the basic length scale and κ as the energy scale, we can define dimensionless, reduced physical quantities

$$\tilde{s} \equiv s/R, \tag{10}$$

$$\tilde{r} \equiv r/R, \tag{11}$$

$$\tilde{\sigma} \equiv \sigma R^2/\kappa, \tag{12}$$

$$\tilde{E} \equiv E/4\pi\kappa. \tag{13}$$

The reduced energy of the un-adhered portion of the membrane can then be written as

$$\Delta\tilde{E}_{\rm free} = \int_0^{\tilde{S}} {\rm d}\tilde{s} \left\{ \frac{\tilde{r}}{2}\left[\frac{{\rm d}\psi}{{\rm d}\tilde{s}} + \frac{\cos\psi}{\tilde{r}}\right]^2 + \tilde{\sigma}\tilde{r} - \sqrt{2\tilde{\sigma}}\cos\psi \right\}, \tag{14}$$

which needs to be minimized with respect to $\psi(\tilde{s})$ with the constraint

$$\frac{{\rm d}\tilde{r}}{{\rm d}\tilde{s}} = -\sin\psi(\tilde{s}), \tag{15}$$

a reduced version of Eq. (3).

We take the Lagrangian–Hamiltonian dynamics approach in solving the minimization problem required, an approach that has been well documented in Refs. [27] and [33] for similar problems. We first introduce an effective Lagrangian function

$$\begin{aligned} L = {} & \frac{\tilde{r}}{2}\left[\frac{{\rm d}\psi}{{\rm d}\tilde{s}} + \frac{\cos\psi}{\tilde{r}}\right]^2 + \tilde{\sigma}\tilde{r} - \sqrt{2\tilde{\sigma}}\cos\psi \\ & + \lambda(\tilde{s})[\dot{\tilde{r}} + \sin\psi(\tilde{s})], \end{aligned} \tag{16}$$

where $\lambda(\tilde{s})$ is a Lagrangian multiplier function to be determined below, and a dotted symbol represents a derivative with respect to $\tilde{s}$. Effective canonical momenta

$$P_\psi(\tilde{s}) \equiv \frac{\partial L}{\partial\dot{\psi}} = \tilde{r}(\dot{\psi} + \frac{\cos\psi}{\tilde{r}}), \tag{17}$$

$$P_r(\tilde{s}) \equiv \frac{\partial L}{\partial\dot{\tilde{r}}} = \lambda(\tilde{s}). \tag{18}$$

can then be introduced. Using the effective Lagrangian, we can define an effective Hamiltonian

$$\begin{aligned} H = {} & P_\psi\dot{\psi} + P_r\dot{\tilde{r}} - L \\ = {} & \frac{P_\psi^2}{2\tilde{r}} - \frac{P_\psi\cos\psi}{\tilde{r}} - \tilde{\sigma}\tilde{r} + \sqrt{2\tilde{\sigma}}\cos\psi - P_r\sin\psi. \end{aligned} \tag{19}$$

Hamilton's equations of motion yield four first-order differential equations to be solved for four functions $\tilde{r}(\tilde{s}), \psi(\tilde{s}), P_r(\tilde{s})$, and $P_\psi(\tilde{s})$, which are

$$\frac{{\rm d}\psi}{{\rm d}\tilde{s}} = \frac{P_\psi}{\tilde{r}} - \frac{\cos\psi}{\tilde{r}}, \tag{20}$$

$$\frac{{\rm d}\tilde{r}}{{\rm d}\tilde{s}} = -\sin\psi, \tag{21}$$

$$\frac{{\rm d}P_\psi}{{\rm d}\tilde{s}} = -\frac{P_\psi\sin\psi}{\tilde{r}} + P_r\cos\psi + \sqrt{2\tilde{\sigma}}\sin\psi, \tag{22}$$

$$\frac{{\rm d}P_r}{{\rm d}\tilde{s}} = \frac{P_\psi^2/2 - P_\psi\cos\psi}{\tilde{r}^2} + \tilde{\sigma}. \tag{23}$$

These four equations need to be amended by four initial conditions for a unique trajectory in $\tilde{s}$. We already have Eq. (8) for ψ so

$$\tilde{r}(0) = \cos\alpha \tag{24}$$

according to the geometry described in Fig. 1. We also use two initial parameters, ξ and ζ

$$P_\psi(0) = \xi, \quad P_r(0) = \zeta \tag{25}$$

in our calculation. Once ξ, ζ, and $\tilde{S}$ are given, the solution to the differential equations gives trajectories of the four functions from $\tilde{s} = 0$ to $\tilde{s} = \tilde{S}$.

The parameters ξ and ζ are determined from the two final conditions at $\tilde{s} = \tilde{S}$. One of them is a mirror boundary condition

$$\psi(\tilde{S}) = 0 \tag{26}$$

imposed in such a way that the shape curve is symmetric at $\tilde{s} = \tilde{S}$; this is valid in two cases: the single sphere adsorption problem where $\tilde{S} = \infty$ and the double sphere adsorption problem where $\tilde{S}$ represents the mid-point between two spheres (see Subsection 3.1). The other condition is the fact that the radius of the tube at $\tilde{s} = \tilde{S}$, $\tilde{r}(\tilde{S})$, is an independent adjustable parameter that can be used to minimize the entire energy. As such, the constraint in Eq. (15) should be lifted exactly at $\tilde{s} = \tilde{S}$, in other words, $\lambda(\tilde{S}) = 0$, or according to Eq. (18)

$$P_r(\tilde{S}) = 0. \tag{27}$$

To generate a trajectory, i.e., the shape curve for given $\tilde{\sigma}$ and α, we numerically solve Eqs. (20)–(23) with an implementation of the forth order Runge–Kutta method.[35] We took a step size $h = 0.0001$ for $\tilde{s}$ to carry the integration forward from $\tilde{s} = 0$ to $\tilde{s} = \tilde{S}$. A shooting method has been used to match the initial conditions ξ and ζ against the final conditions in Eqs. (26) and (27). The result is a numerical table, where the energy difference $\Delta\tilde{E}_{\rm free}$ is listed as a function of $\tilde{\sigma}$, α, and $\tilde{S}$

$$\Delta\tilde{E}_{\rm free} = \Delta\tilde{E}_{\rm free}(\tilde{\sigma}, \alpha, \tilde{S}). \tag{28}$$

3. Results and discussion

3.1. Two spheres in a tube

In this subsection, we consider the scenario where two spheres are confined in a tube. The system can be treated by imaginarily separating the middle portion, between the two vertical diameters in Fig. 2, from the rest. While the free portion of the tube is described by $\Delta E_{\rm free}(\tilde{\sigma}, \alpha, \tilde{S})$ discussed above, the adhered portion is assumed to interact with the sphere's surface by an attraction energy per unit area, w (negtive). The same parameter has been introduced recently in a number of closely related systems.[15,23,24,26–28,30]

Using a reduced

$$\tilde{w} \equiv wR^2/\kappa, \tag{29}$$

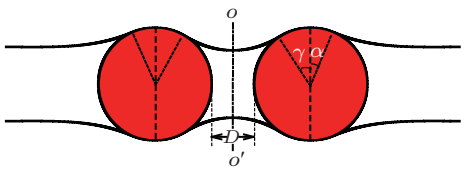


Fig. 2. (color online) Schematic representation of the system of two spheres confined in a co-axial soft tube. Two wrapping angles, γ and α, for the wrapped portions on the left and right hemisphere of the sphere on the right-hand side, are independently used in the text. The distance between the surfaces of the two spheres, D, is related to the total path length S of the non-adhered membrane shape, from the contact point to the middle point.

we can write the total energy for the remaining part, which is identical to the single sphere in a tube[15]

$$\begin{aligned}&\Delta\tilde{E}_{\rm I}(\tilde{\sigma},\tilde{w};\alpha)\\&=\int_0^{\tilde{S}}{\rm d}\tilde{s}\left\{\frac{\tilde{r}}{2}\left[\frac{{\rm d}\psi}{{\rm d}\tilde{s}}+\frac{\cos\psi}{\tilde{r}}\right]^2+\tilde{\sigma}\tilde{r}-\sqrt{2\tilde{\sigma}}\cos\psi\right\}\\&+(2+\tilde{\sigma}+\tilde{w})\sin\alpha-\sqrt{2\tilde{\sigma}}\sin\alpha.\end{aligned}\tag{30}$$

The energy of the middle portion has the same structure as the energy in Eq. (28), but with the wrapping angle α replaced by γ. Including the adhesion energy, we write

$$\Delta\tilde{E}'_{\rm I}(\tilde{\sigma},\tilde{w};\gamma,\tilde{S})=\Delta\tilde{E}_{\rm free}(\tilde{\sigma},\gamma;\tilde{S})+\Delta\tilde{E}_{\rm ad}(\tilde{\sigma},\tilde{w};\gamma),\tag{31}$$

where the last term is already expressed in Eq. (30). For the entire system, the task then becomes minimizing the total energy

$$\Delta\tilde{E}_{\rm II}(\tilde{\sigma},\tilde{w};\alpha,\gamma,\tilde{S})=\Delta\tilde{E}_{\rm I}(\tilde{\sigma},\tilde{w};\alpha)+\Delta\tilde{E}'_{\rm I}(\tilde{\sigma},\tilde{w};\gamma,\tilde{S}),\tag{32}$$

with respect to $\alpha,\gamma,\tilde{S}$ as variables.

Because of the sum of the two independent energy contributions in the last expression, in most cases discussed below, the $\Delta\tilde{E}_{\rm I}(\tilde{\sigma},\tilde{w};\alpha)$ and $\Delta\tilde{E}'_{\rm I}(\tilde{\sigma},\tilde{w};\gamma,\tilde{S})$ can be minimized with respect to α and γ, $\tilde{S}$ respectively.

The minimization of the former one has been fully discussed by Chen *et al.*[15] In this paper, we just examine a few typical energy curves in Fig. 3 in the following discussion, which shows $\Delta\tilde{E}_{\rm I}(\tilde{\sigma},\tilde{w};\alpha)$ as a function of α for various $\tilde{\sigma}$ at a given $\tilde{w}$.

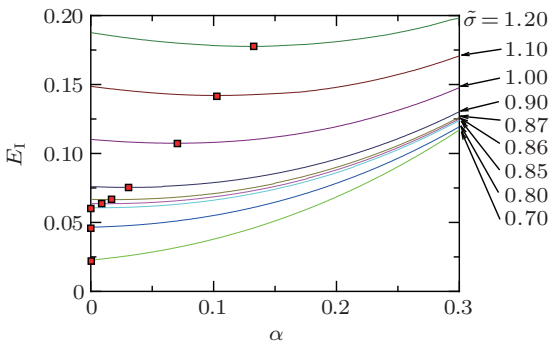


Fig. 3. (color online) Examples of the reduced energy $\Delta\tilde{E}_{\rm I}$ (Eq. 30) for various values of $\tilde{\sigma}$ as a function of the wrapping angle α, at $\tilde{w}=-0.25$. Squares represent the locations of minima, $\alpha_{\rm m}$ in these curves.

Numerically, the latter is determined from searching through the energy corresponding to the variable space of these two variables; the location of the energy minimum, $\gamma_{\rm m}$ and $\tilde{S}_{\rm m}$, is then considered in constructing the structures in Fig. 4(a) and the phase diagram in Fig. 4(b). In certain regions of the physical parameters, $\tilde{\sigma}$ and $\tilde{w}$, for finite $\tilde{S}$, two branches of the energy curves exist. One branch corresponds to a shallow shape curve in the middle portion of the soft tube with a small $\gamma_{\rm m}$ and the other a deep curve with a large $\gamma_{\rm m}$. Most phase boundaries in Fig. 4(b) are determined by the comparison of the total minimized energies of different branches, except for the $\rm II_1$–$\rm II_4$ boundary, which will be discussed in more detail near the end of this subsection.

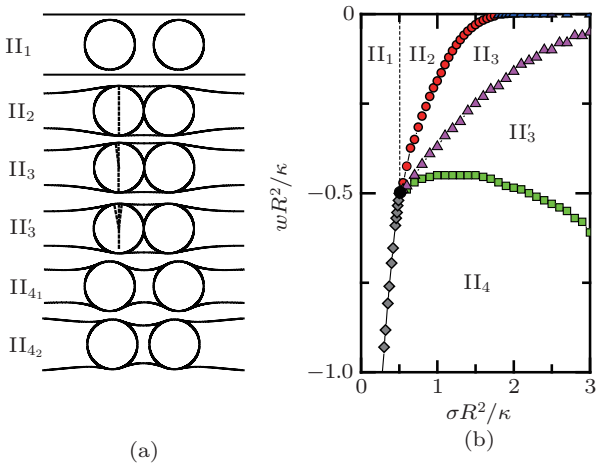


Fig. 4. (color online) Structures (a) and phase diagram (b) determined in this work for the system of two spheres confined inside a soft tube. The six representative structures in panel (a) are produced from the numerical solution for $[\tilde{\sigma},\tilde{w}]=[0.4,-0.25],[1.0,-0.10],[1.0,-0.25],[1.0,-0.43],[1.0,-1.00]$, and $[0.4,-1.00]$, respectively. The contact angles of $\rm II_2$, $\rm II_3$, $\rm II'_3$ are marked with short dashed lines to indicate the slight differences.

On the basis of a given shape curve, we can evaluate the reduced surface-to-surface distance between two spheres

$$\tilde{D}\equiv D/R,\tag{33}$$

as a function of γ and $\tilde{S}$ (see Fig. 2 for the relation between these parameters)

$$\tilde{D}(\gamma,\tilde{S})=2\left(\int_0^{\tilde{S}}\cos\psi{\rm d}\tilde{s}+\sin\gamma-1\right).\tag{34}$$

The optimized distance

$$\tilde{D}_{\rm m}=\tilde{D}(\gamma_{\rm m},\tilde{S}_{\rm m})\tag{35}$$

can then be calculated, which is a quantity that we discuss below.

Multiple stable phases emerge from this analysis. In phase $\rm II_1$, $a>R$, the two spheres can move freely inside the tube, while the diameter of the soft tube remains constant at a. The distance between two spheres are not required to be fixed at any given value by the energy minimum.

Phase II_2 is in a region where $\tilde{\sigma} > 1/2$ or $a < R$. There is no adhesion area between the spheres and the soft tube along the entire tube ($\alpha_\mathrm{m} = \gamma_\mathrm{m} = 0$). The shape of the tube segment between the two spheres is weakly distorted and bent towards the axis, although the shape distortion is not clearly visible in the II_2 plot of Fig. 4(a). The two spheres are confined next to each other with contacting spherical surfaces ($\tilde{D}_\mathrm{m} = 0$). Figures 5(a) and 5(b) show $\alpha_\mathrm{m} = \gamma_\mathrm{m} = \tilde{D}_\mathrm{m} = 0$ and $\tilde{S}_\mathrm{m}$ slightly above 1 in phase II_2. The phase transition between II_2 and II_3 is mainly driven by a continuous adhesion transition associated with the wrapping angle α, which can be further explained by a few typical energy curves. Figure 3 shows $\Delta\tilde{E}_\mathrm{I}(\tilde{\sigma}, \tilde{w}; \alpha)$ as a function of α for various $\tilde{\sigma}$ at a given $\tilde{w} = -0.25$. In a system with $\tilde{\sigma} < 0.85$, the energy minimum corresponds to $\alpha_\mathrm{m} = 0$ hence no common contact area, reflecting the fact that there is no adhesion between the spherical surface and the membrane tube. Note that this includes two types of conformations, $\tilde{\sigma} \leq 1/2$ and $1/2 < \tilde{\sigma} \leq 0.85$, corresponding to the phases II_1 and II_2 as discussed above.

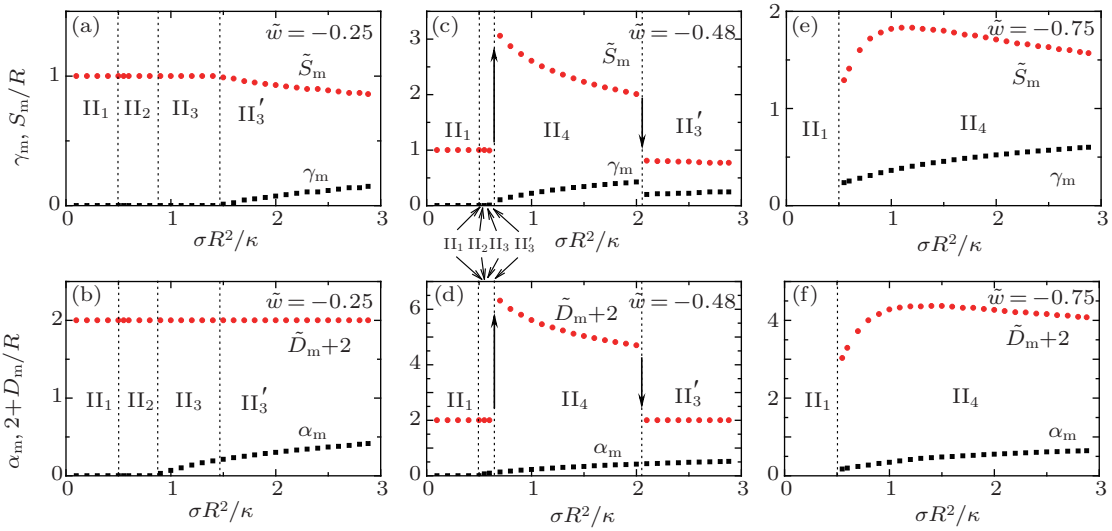


Fig. 5. (color online) Wrapping angles α_m and γ_m, reduced center-to-center distance between two confined spheres $2 + D_\mathrm{m}/R$, and reduced membrane segment length S_m/R, as functions of the reduced surface tension $\sigma R^2/\kappa$ for $\tilde{w} = -0.25$ [in plots (a) and (b)], $\tilde{w} = -0.48$ [in plots (c) and (d)], and $\tilde{w} = -0.75$ [in plots (e) and (f)]. Phase boundaries are indicated by vertical dashed lines. By adjusting the stretching force along the axis of the membrane tube hence changing σ, D_m can be directly probed in an experiment.

Further crossing the transition point at $\tilde{\sigma}^* = 0.85$ [i.e., the boundary indicated by circles in Fig. 4(b)], we can identify a nonzero wrapping angle α_m where the energy in Fig. 3 shows a minimum. Using squares we show in Fig. 5(b) how the energetically preferred wrapping angle α_m changes as a function of the reduced surface tension $\tilde{\sigma}$, for $\tilde{w} = -0.25$. The entire II_2–II_3 curve in Fig. 4(b) is numerically determined by the first occurrence of $\alpha_\mathrm{m}(\tilde{\sigma}, \tilde{w}) \neq 0$. In addition, in this phase, the wrapping angle γ_m is still zero, indicating no adhesion in the middle portion of the tube. The shape of the tube segment between the two spheres is further distorted, however, there still remains a weak effect, which cannot be clearly seen in the II_3 plot of Fig. 4(a). Corresponding to the weak distortion, the energy of the middle tube segment prefers two spheres in contact with each other ($\tilde{D}_\mathrm{m} = 0$). Figures 5(a) and 5(b) show $\alpha_\mathrm{m} \neq 0$, $\gamma_\mathrm{m} = \tilde{D}_\mathrm{m} = 0$, and $\tilde{S}_\mathrm{m}$ slightly above 1 in phase II_3.

Both stronger adhesion energy $|\tilde{w}|$ and stronger reduced surface tension $\tilde{\sigma}$ can drive the middle portion of the soft tube to make a continuous adhesion transition, characterized by the appearance of a nonzero wrapping angle γ_m beyond the II_3–II_3' phase boundary shown in Fig. 4(b). This transition is very similar to the adhesion mechanism for the II_2–II_3 transition and is of a continuous nature; the only difference is that the involved middle tube segment has a finite length. The surface-to-surface distance of the two spheres is still preferred to be zero in phase II_3', shown in Fig. 5(b). From the same plot, we can see that the wrapping angle α_m varies smoothly crossing the phase boundary. In the preliminary report of a study of the current model,[15] the difference between II_3 and II_3' phases was missed and unidentified. As the adhesion energy $|\tilde{w}|$ further increases, another branch of the energy curve becomes dominant, driving the system to undergo a discontinuous II_3'–II_4 transition, shown in Fig. 4(b) by squares. In phase II_4, a much larger wrapping angle γ_m is stabilized together with a significant distortion of the membrane shape between the two spheres [see the illustration labeled II_4 in

Fig. 4(a)]. Such a larger γ_m is preferred by the adhesion energy $\Delta\tilde{E}_{\rm ad}(\tilde{\sigma},\tilde{w};\gamma)$ with a strong $|\tilde{w}|$. The price to pay is a larger distortion energy associated with a longer tube segment between the two spheres. Crossing the discontinuous II_3'–II_4 boundary, $\alpha_{\rm m}$ remains continuous but $\gamma_{\rm m}$ undergoes a jump, shown in Figs. 5(d) and 5(c), respectively; the most significant property of phase II_4 is a large $D_{\rm m}$, shown in Figs. 5(d) and 5(f), which is no longer 0 as in the II_2, II_3, and II_3' phases.

Finally, the discontinuous II_1–II_4 phase boundary is determined by requiring

$$\Delta\tilde{E}_{\rm I}(\tilde{\sigma},\tilde{w};\alpha_{\rm m})+\Delta\tilde{E}_{\rm I}'(\tilde{\sigma},\tilde{w};\gamma_{\rm m},\tilde{S}_{\rm m})=0. \tag{36}$$

To obtain the energy of a II_4 phase, we enforce an adhered structure, shown by the II_4 plot in Fig. 4(a) and numerically determined by the energy minima for the $\Delta E_{\rm I}$ and $\Delta E_{\rm I}'$ parts separately. The corresponding optimized $\alpha_{\rm m},\gamma_{\rm m}$, and $\tilde{S}_{\rm m}$ are all functions of $\tilde{\sigma}$ and $\tilde{w}$. The above equation then describes a phase boundary in terms of $\tilde{\sigma}$ and $\tilde{w}$, beyond which the phase II_4 is stable and has a negative total energy. Note that the II_1–II_4 boundary is different from the I_1–I_3 boundary in the single sphere phase diagram in Ref. [15] where the first term in the above equation is considered separately.

3.2. The N spheres in a soft tube

The above analysis can be readily generalized to the system of N identical spheres confined in a soft tube. Except for the desorbed state (N_1) where these N particles can freely move in the tube with no specific structure, all other possible configurations in Fig. 6(a) have $N-1$ inner tube portions in the system. Due to the symmetry of the system and the identical particles, we can assume that these portions have identically the same structure. Following the same analysis in the beginning of the last subsection, we write the total energy of the system

$$\begin{aligned}&\Delta\tilde{E}_N(\tilde{\sigma},\tilde{w};\alpha,\gamma,\tilde{S})\\&=\Delta\tilde{E}_{\rm I}(\tilde{\sigma},\tilde{w};\alpha)+(N-1)\Delta\tilde{E}_{\rm I}'(\tilde{\sigma},\tilde{w};\gamma,\tilde{S}).\end{aligned} \tag{37}$$

The energy needs to be minimized with respect to α, γ, $\tilde{S}$ as variables.

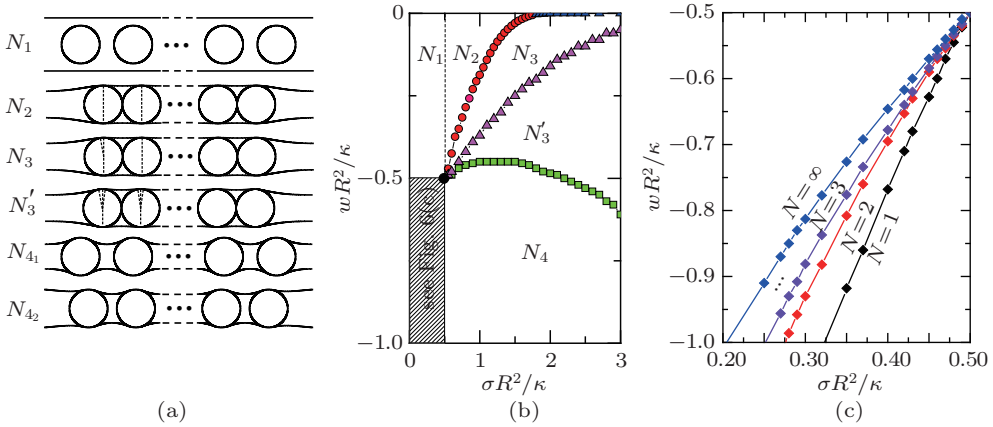


Fig. 6. (color online) Structures (a), phase diagram (b), and an enlarged area of the phase diagram (c), determined in the current work for the system of N spheres confined inside a soft tube. The phase boundaries underlying circles as well as triangles are continuous, and squares as well as diamonds are discontinuous. The six representative structures in panel (a) are produced from the numerical solution for $[\tilde{\sigma},\tilde{w}]=[0.4,-0.25],[1.0,-0.10],[1.0,-0.25],[1.0,-0.43],[1.0,-1.00]$, and $[0.4,-1.00]$, respectively. The contact angles of N_2, N_3, N_3' are marked with short dashed lines to indicate the slight differences.

Most results in the above section can be directly used for the case of N particles. For example, the continuous N_2–N_3, continuous N_3–N_3', and discontinuous N_3'–N_4 phase boundaries [see Fig. 6(b)] remain identically the same as the II_2–II_3, II_3–II_3', and II_3'–II_4 phase boundaries [see Fig. 4(b)]. The inner portions can be characterized by the wrapping angle γ and surface-to-surface distance D, which have the same behavior as those described in Fig. 5.

One important difference from Fig. 4(b), though, is the location of the discontinuous phase boundary N_1–N_4 in Fig. 6(b), which is labeled by the shaded area and further illustrated in an enlarged version in Fig. 6(c). The boundary is determined from

$$\Delta\tilde{E}_{\rm I}(\tilde{\sigma},\tilde{w};\alpha_{\rm m})+(N-1)\Delta\tilde{E}_{\rm I}'(\tilde{\sigma},\tilde{w};\gamma_{\rm m},\tilde{S}_{\rm m})=0, \tag{38}$$

where $\alpha_{\rm m},\gamma_{\rm m}$, and $\tilde{S}_{\rm m}$ are all functions of $\tilde{\sigma}$ and $\tilde{w}$, minimized in the previous two subsections to yield energy minima in the outer and inner portions of the soft tube. The $N-1$ prefactor renders different N_1–N_4 phase boundaries as a function of N, which are plotted in Fig. 6(c).

4. Summary

In this paper, we describe the detailed theoretical procedure used to determine the once reported phase behavior of

confined spherical particles in a soft tube.[15] A new phase boundary has been amended in Fig. 4(b) and a number of physical properties have now been discussed in this paper. Qualitatively, because of the similarity between Figs. 6(b) and 4(b), our predictions on the phase behavior of this system can be experimentally probed by any number of confined spheres. In a typical experimental system, w, R, and κ are all fixed physical parameters. Assume now that the formation of a membrane tube is yielded from pulling one end of the long tube by a force. The so-called surface tension, σ, is directly related to the force hence can be experimentally manipulated. As a function of σ with fixed w, R, and κ, we can examine the phase behavior through a signatural force–distance curve, where the distance is between the pulling tip of the tube membrane and the stemming (starting) part of the vesical. Crossing each phase boundary, an abrupt step or change of slope can be observed in the force–distance curve, corresponding to a first-order or second-order phase transition.

Acknowledgments

We thank Jeff Z. Y. Chen for useful comments and discussion.

References

[1] Dai J and Sheetz M P 1999 *Biophys. J.* **77** 3363
[2] Borghi N, Rossier O and Brochard-Wyart F 2003 *Europhys. Lett.* **64** 837
[3] Karlsson A, Karlsson R, Karlsson M, Cans A F, Stromberg A, Ryttsen F and Orwar O 2001 *Nature* **409** 150
[4] Roux A, Cappello G, Cartaud J, Prost J, Goud B and Bassereau P 2002 *Proc. Natl. Acad. Sci. USA* **99** 5394
[5] Tsafrir I, Caspi Y, Guedeau-Boudeville M A, Arzi T and Stavans J 2003 *Phys. Rev. Lett.* **91** 138102
[6] Campas O, Leduc C, Bassereau P, Casademunt J, Joanny J F and Prost J 2008 *Biophys. J.* **94** 5009
[7] Kuhnl W, Piry A, Kaufmann V, Grein T, Ripperger S and Kulozik U 2010 *J. Membr. Sci.* **352** 107
[8] Springer F, Carretier E, Veyret D, Dhaler D and Moulin P 2011 *Chem. Eng. Process.* **50** 904
[9] Tokarz M, Akerman B, Olofsson J, Joanny J F, Dommersnes P and Orwar O 2005 *Natl. Acad. Sci. USA* **102** 9127
[10] Tokarz M, Hakonen B, Dommersnes P, Orwar O and Akerman B 2007 *Langmuir* **23** 7652
[11] Hurtig J and Orwar O 2008 *Soft Matter* **4** 1515
[12] Brochard-Wyart F, Tanaka T, Borghi N and Degennes P G 2005 *Langmuir* **21** 4144
[13] Avramova K and Milchev A 2006 *J. Chem. Phys.* **124** 024909
[14] Chen J Z Y 2007 *Phys. Rev. Lett.* **98** 088302
[15] Chen J Z Y, Liu Y and Liang H J 2009 *Phys. Rev. Lett.* **102** 168103
[16] Tu Z C 2013 *Chin. Phys. B* **22** 028701
[17] Peng Y G and Zheng Y J 2011 *Acta Phys. Sin.* **60** 088701 (in Chinese)
[18] Niu Y Q, Wei W, Zheng B, Zhang C X and Meng Q T 2013 *Chin. Phys. B* **22** 128701
[19] Helfrich W and Servuss R M 1984 *Nuovo Cimento D* **3D** 137
[20] Helfrich W 1973 *Z. Naturforsch C* **28** 693
[21] Derenyi I, Julicher F and Prost J 2002 *Phys. Rev. Lett.* **88** 238101
[22] Seifert U, Berndl K and Lipowsky R 1991 *Phys. Rev. A* **44** 1182
[23] Seifert U and Lipowsky R 1990 *Phys. Rev. A* **42** 4768
[24] Seifert U 1991 *Phys. Rev. A* **43** 6803
[25] Deserno M and Gelbart W M 2002 *J. Phys. Chem. B* **106** 5543
[26] Weikl T R 2003 *Eur. Phys. J. E* **12** 265
[27] Deserno M 2004 *Phys. Rev. E* **69** 031903
[28] Deserno M 2004 *J. Phys.: Condens. Matter* **16** S2061
[29] Das S and Du Q 2008 *Phys. Rev. E* **77** 011907
[30] Chen J Z Y and Mkrtchyan S 2010 *Phys. Rev. E* **81** 041906
[31] Cao S, Wei G and Chen J Z Y 2011 *Phys. Rev. E* **84** 050901
[32] Chen J Z Y 2012 *Phys. Rev. E* **85** 061910
[33] Seifert U 1997 *Advances in Physics* **46** 13
[34] Muller M, Katsov K and Schick M 2006 *Phys. Rep.* **434** 113
[35] Press W H, Teukolsky S A,Vetterling W T and Flannary B P 1992 *Numerical Recipes in C* (2nd edn.) (Cambridge: Cambridge University Press) p. 757